

Structural Dynamics of Bismuth Triiodide in Solution Triggered by Photoinduced Ligand-to-Metal Charge Transfer

Eun Hyuk Choi,^{†,‡,⊥} Doo-Sik Ahn,^{†,‡,⊥} Sungjun Park,^{†,‡} Changwon Kim,^{†,‡} Chi Woo Ahn,^{†,‡} Siin Kim,^{†,‡} Minseo Choi,^{†,‡} Cheolhee Yang,[‡] Tae Wu Kim,[‡] Hosung Ki,[‡] Jungkweon Choi,^{†,‡,⊥} Martin Nors Pedersen,[§] Michael Wulff,[§] Jeongho Kim,[#] and Hyotcherl Ihee^{*,†,‡,⊥}

[†]Department of Chemistry and KI for the BioCentury, Korea Advanced Institute of Science and Technology (KAIST), Daejeon 34141, Republic of Korea

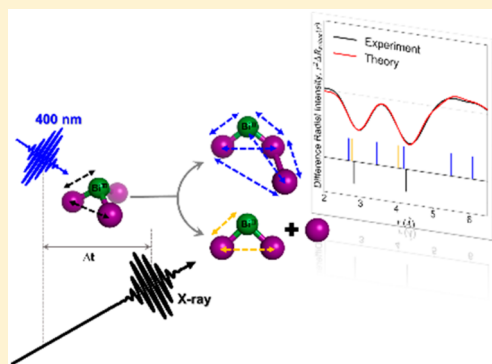
[‡]Center for Nanomaterials and Chemical Reactions, Institute for Basic Science (IBS), Daejeon 34141, Republic of Korea

[#]Department of Chemistry, Inha University, 100 Inha-ro, Nam-gu, Incheon 22212, Republic of Korea

[§]European Synchrotron Radiation Facility (ESRF), 38000 Grenoble Cedex 9, France

Supporting Information

ABSTRACT: Bismuth triiodide, BiI₃, is one of the simplest bismuth halides, which have recently attracted considerable attention because of their promising properties. Here, we investigate the structural dynamics of a photoinduced reaction of BiI₃ in solution phase using time-resolved X-ray liquidography (TRXL) and density functional theory (DFT) and time-dependent DFT (TDDFT) calculations. The photoreaction was initiated by excitation at 400 nm, which corresponds to the ligand-to-metal charge-transfer transition. The detailed structures and kinetic profiles of all relevant intermediate species from the TRXL data show that the trigonal planar structure of BiI₃, which is predicted to be the most stable structure of the lowest excited state by TDDFT calculation, was not observed, and the photoreaction proceeds via two parallel pathways within the time resolution of 100 ps: (i) isomer formation to produce *iso*-BiI₂-I, which relaxes back to the ground-state structure, and (ii) dissociation into BiI₂[•] and I[•] radicals, which nongeminately recombine to generate ground-state BiI₃ and I₂.



Metal halides, a class of polyhalogenated compounds, have attracted much interest because of their remarkable photophysical and photochemical properties and their controllability with different ligands.^{1–3} In particular, light-driven processes of metal halides in the liquid solution phase have been investigated intensely because of fundamental interest and their wide applicability for various optoelectronic materials.^{4–9} However, because of the presence of heavy atoms, photoexcited metal halides undergo complex relaxation pathways, both radiative and nonradiative, making it challenging to elucidate the detailed mechanisms of photoinduced processes. Among metal halides, bismuth-based compounds have come into the spotlight in many fields of chemistry and physics for their low toxicity and low cost compared with other metal halide compounds.¹⁰ For example, bismuth halides have recently been proposed as one of the most promising lead-free metal halide materials for solid-state perovskite photovoltaics.^{11–14} In addition, they are good catalysts for various organic reactions, including Diels–Alder reactions and acylation reactions.^{15,16} Bismuth triiodide, BiI₃, is the simplest bismuth halide and can serve as an excellent model system to investigate the characteristics of bismuth halides. Initially, Molnar et al. pioneered the detailed molecular

structure of BiI₃ using gas-phase electron diffraction combined with vibrational spectroscopy.¹⁷ While most of previous studies of BiI₃ have focused on the characterization of the structure and photophysical properties of solid-state BiI₃,¹⁸ Horvath et al. have demonstrated, in their studies on BiI_n^{(n–3)–}, ultraviolet (UV) photoexcitation of BiI₃ in solution with the solvent of acetonitrile, subsequently leading to photoredox decomposition generating molecular iodine as a final product.^{19,20} To the best of our knowledge, however, the mechanism of the UV-initiated photoreaction of BiI₃ in the liquid solution phase has never been investigated. In particular, the reaction intermediates involved in the photoreaction of BiI₃ and their detailed kinetics have not been determined yet. Although crystalline BiI₃ in the solid phase has been a hot topic because of their technological applications, it is necessary to elucidate the photochemical behavior of a constituent unit cell, that is, solvated molecular BiI₃ in solution, for a better understanding of the optoelectronic properties of the material.

Received: February 7, 2019

Accepted: March 5, 2019

Published: March 5, 2019

Previously, the major intermediates generated by photoexcitation of polyhalogenated compounds were identified by time-resolved spectroscopic and X-ray scattering experiments.^{21–23} In particular, isomeric species of polyhalogenated compounds have been identified as key intermediates involved in the relaxation of dissociative excited states.^{24,25} For example, Tarnovsky and co-workers have studied ultrafast photoisomerization of various polyhalide compounds in solution by using ultrafast time-resolved spectroscopy and quantum calculations.²⁶ Recently, time-resolved X-ray solution scattering (TRXSS), also known as time-resolved X-ray liquidography (TRXL), has been widely used to directly capture the structures of transient intermediates.^{27–31} Using TRXL, Ahn et al. recently reported a global scheme for the reaction pathways of UV-excited CHI_3 in cyclohexane and, especially, identified an isomeric reaction intermediate, $\text{iso-CHI}_2\text{-I}$.³² In addition, using TRXL, Marcellini and co-workers observed the solvent-dependent formation of two types of isomeric species of CH_2IBr .³³

In this work, we investigate the photoinduced structural dynamics of BiI_3 in acetonitrile by TRXL. Upon UV excitation, BiI_3 is expected to undergo photochemical reactions including dissociation, bond formation, and isomer formation. Three possible candidate intermediates based on the literature and our theoretical predictions by quantum calculation are presented in Figure 1. In the present study, we employ the excitation at 400 nm, which excites the lowest transition of BiI_3 in acetonitrile solution. This transition has been assigned to the LMCT transition, which generally induces intramolecular photoredox reactions with the metal center reduced and ligands oxidized.

Experimental scattering curves measured at various time delays from a TRXL experiment are shown in Figure 2a, together with theoretical scattering curves that were fit to the experimental scattering curves using the best kinetic model, which will be discussed below.

It can be seen that the experimental and theoretical curves are in good agreement with each other, indicating the relevance of the kinetic model. In Figure 2b, difference radial intensities, $r^2\Delta R(r)$, obtained by sine-Fourier transform of the difference scattering curves in Figure 2a are shown together with theoretical $r^2\Delta R(r)$ curves that well reproduce the experimental ones. The scattering signal of a solution sample can be decomposed into (i) the solute-only term, (ii) the cage term, and (iii) the solvent-only term, as shown in Figures S1–S3 in the Supporting Information. Note that, as shown in Figure S1, the total scattering intensity of the solution sample is dominated by the solute-only term because of large atomic form factors of the heavy atoms in the solute molecule and the substantial structural changes of the solute molecule.

To find the best kinetic model that can describe the mechanism of photoreaction of BiI_3 , we examined four candidate reaction pathways: (i) formation of trigonal planar BiI_3 with D_{3h} symmetry, which is predicted as the most stable structure of the lowest singlet excited state S_1 according to our time-dependent density functional theory (TDDFT) calculations (which will be discussed below); (ii) formation of dissociation fragments ($\text{BiI}_2\cdot + \text{I}\cdot$); (iii) formation of an isomer, $\text{iso-BiI}_2\text{-I}$, as observed in photoreactions of various polyhalogenated compounds; and (iv) formation of a mixture of dissociation fragments ($\text{BiI}_2\cdot + \text{I}\cdot$) and $\text{iso-BiI}_2\text{-I}$. As an example of examining these candidate pathways, we show in Figure 3 the results of the fitting analysis for the experimental

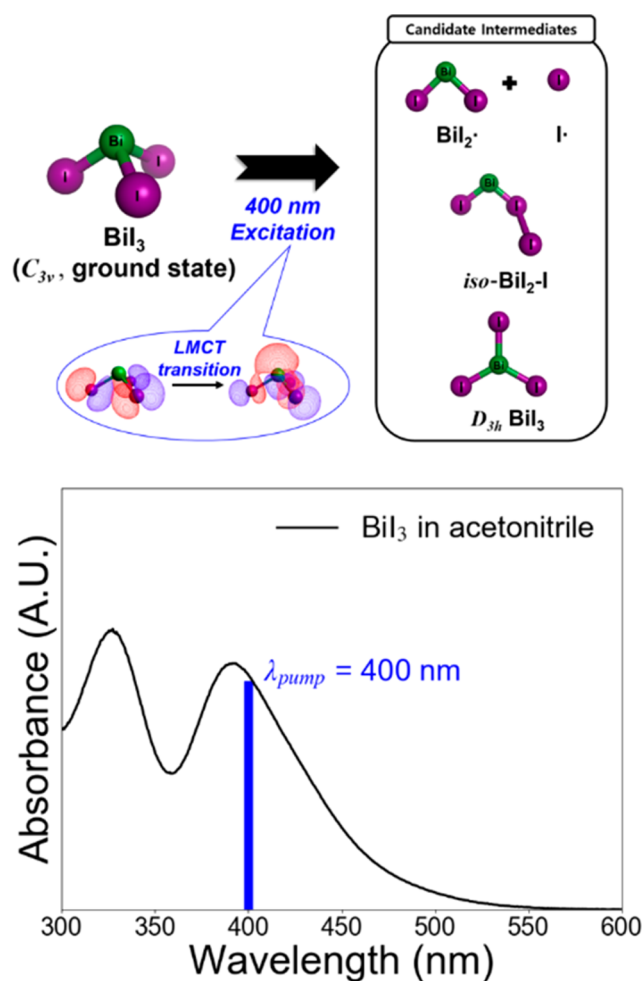


Figure 1. Candidate intermediates of BiI_3 in acetonitrile upon 400 nm excitation of LMCT transition and the steady-state absorption spectrum of BiI_3 in acetonitrile.

scattering curve at 100 ps. The candidate pathway (i), that is, the formation of trigonal planar BiI_3 with D_{3h} symmetry, exhibits a marked discrepancy between the experimental curve and the theoretical curve, giving the highest χ^2 value. The fit curve of the candidate pathway (ii) agrees well with the experimental curve up to $q = 6 \text{ \AA}^{-1}$ but shows deviation at high q values of $6\text{--}9 \text{ \AA}^{-1}$. By contrast, the fit curve of (iii) gives slightly better agreement at high q values but deviates significantly in the low q region around $1\text{--}2 \text{ \AA}^{-1}$. The experimental curve is most satisfactorily reproduced with the candidate pathway (iv) that combines pathways (ii) and (iii), indicating that the LMCT transition induced by 400 nm excitation leads to both isomer formation and dissociation of BiI_3 . Accordingly, the theoretical scattering curves shown in Figure 2 were obtained with the kinetic model involving the candidate pathway (iv).

This finding can be more intuitively represented when the scattering intensities in q -space are sine-Fourier transformed into radial intensities in real space. As X-ray crystallography can determine the structure of a crystal in real space, the real space representation of the solution scattering signal directly visualizes the average structure of the solute molecules in solution, even though the solution scattering data are one-dimensional and therefore contain much less structural information than those from X-ray crystallography.^{34,35} To

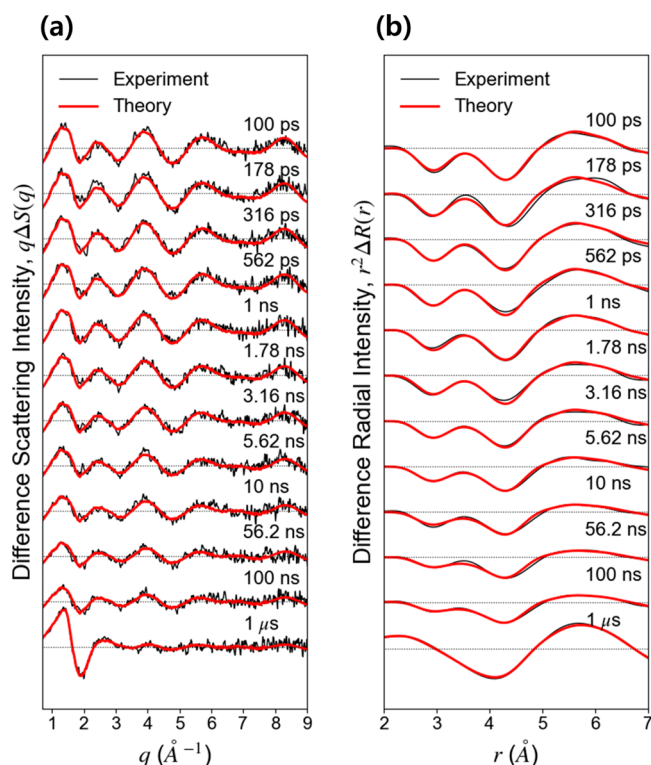


Figure 2. TRXL signals of BiI_3 in acetonitrile measured with excitation at 400 nm. (a) Experimental (black) and theoretical (red) difference scattering curves, $q\Delta S(q)$. (b) Difference radial intensities, $r^2\Delta R(r)$, obtained by sine-Fourier transformation of $q\Delta S(q)$ in panel a.

visualize the structural change of BiI_3 with higher clarity, we focus on the solute-only difference radial intensities, $r^2\Delta R_{\text{solute}}(r)$, at 100 ps. Details of how to extract the solute-only contribution are described in the [Supporting Information](#). In [Figure 4a–d](#), the theoretical $r^2\Delta R_{\text{solute}}(r)$ curves for the four candidate pathways are compared with the experimental $r^2\Delta R_{\text{solute}}(r)$ curve. In [Figure 4e](#), various interatomic distances in the reactant and the candidate photoproducts are indicated by colored arrows, and these interatomic distances are indicated by vertical bars of corresponding colors at the bottom of [Figure 4a–d](#).

For example, ground-state BiI_3 has two types of atomic pair distances: the three equivalent Bi–I bond lengths of 2.82 Å and the three equivalent I··I distances of 4.26 Å. When some of these atomic pair distances are changed in the reaction, negative peaks will be observed at the original values of the interatomic distances in the ground-state BiI_3 , as indicated by downward bars in [Figure 4a–d](#). Indeed, the experimental $r^2\Delta R_{\text{solute}}(r)$ has (i) negative peaks at r values corresponding to the atomic pair distances in the ground-state BiI_3 and (ii) broad positive features around 5–6 Å, which implies that one or more Bi–I distances in the ground-state BiI_3 are changed and new atomic pairs with longer distances are formed in the reaction. For candidate pathway (i) shown in [Figure 4a](#), there are considerable discrepancies between the theoretical and experimental $r^2\Delta R_{\text{solute}}(r)$ as in the reciprocal space representation shown in [Figure 3](#). In particular, theoretical $r^2\Delta R_{\text{solute}}(r)$ for D_{3h} trigonal planar BiI_3 shows two derivative-like features at ~ 3 and ~ 5 Å. These features arise from the Bi–I and I–I distances of D_{3h} trigonal planar BiI_3 , which are longer than those of ground-state BiI_3 , as

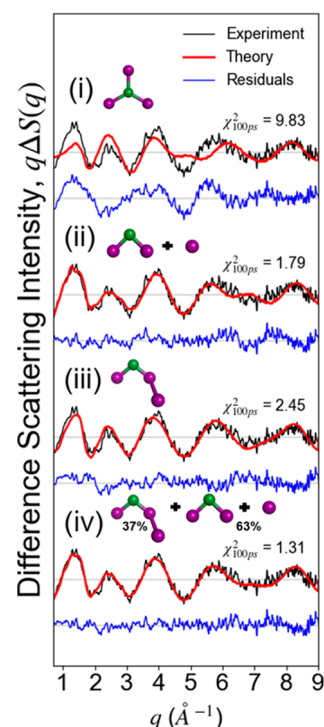


Figure 3. Fits of the difference scattering curve at 100 ps using four candidate pathways: (i) formation of trigonal planar BiI_3 with D_{3h} symmetry, (ii) dissociation fragments ($\text{BiI}_2\cdot + \text{I}\cdot$), (iii) *iso*- $\text{BiI}_2\text{-I}$, and (iv) a mixture of *iso*- $\text{BiI}_2\text{-I}$ and dissociation fragments ($\text{BiI}_2\cdot + \text{I}\cdot$). Experimental (black) and theoretical (red) difference scattering curves, $q\Delta S(q)$, are shown with the residuals (blue) obtained by subtracting the theoretical $q\Delta S(q)$ from the experimental $q\Delta S(q)$. The χ^2 value and the molecular structures of photoproducts are also shown for each candidate pathway. Candidate (iv) gives the best fit.

represented by green upward bars in [Figure 4a](#). For candidate pathway (ii) shown in [Figure 4b](#), the theoretical curve decently reproduces the two negative peaks originating from the depletion of one Bi–I and two I··I distances of ground-state BiI_3 , but it does not describe at all the broad positive feature at distances longer than ~ 5 Å in the experimental $r^2\Delta R_{\text{solute}}(r)$ because two Bi–I and one I··I distances of $\text{BiI}_2\cdot$ are slightly shorter than those of ground-state BiI_3 . For candidate pathway (iii) shown in [Figure 4c](#), the positive and negative features of the theoretical $r^2\Delta R_{\text{solute}}(r)$ are located at the same positions as those of the experimental $r^2\Delta R_{\text{solute}}(r)$ because of longer I··I and Bi··I distances of newly formed *iso*- $\text{BiI}_2\text{-I}$ than those of depleted ground-state BiI_3 , but the intensities of those features in the theoretical and experimental $r^2\Delta R_{\text{solute}}(r)$ do not match each other. In contrast, as shown in [Figure 4d](#), candidate pathway (iv), which combines pathways (ii) and (iii), gives excellent agreement between the experimental and theoretical $r^2\Delta R_{\text{solute}}(r)$, indicating the reaction mechanism involves the two parallel reaction pathways, that is, dissociation and isomer formation.

The reaction mechanism of photoinduced reaction of BiI_3 in acetonitrile and the time-dependent concentrations of all the reactant and photoproduct species determined from the TRXL data are shown in panels (a) and (b) of [Figure 5](#), respectively. According to the TRXL results, $52.6 \pm 0.6\%$ of ground-state $\text{Bi}^{\text{III}}\text{I}_3$ (where the oxidation number of Bi is indicated) is initially excited to the LMCT state, $\text{I-Bi}^{\text{II}}\text{I}_2$, resulting in the reduction of the central Bi^{3+} atom to Bi^{2+} and the oxidation of

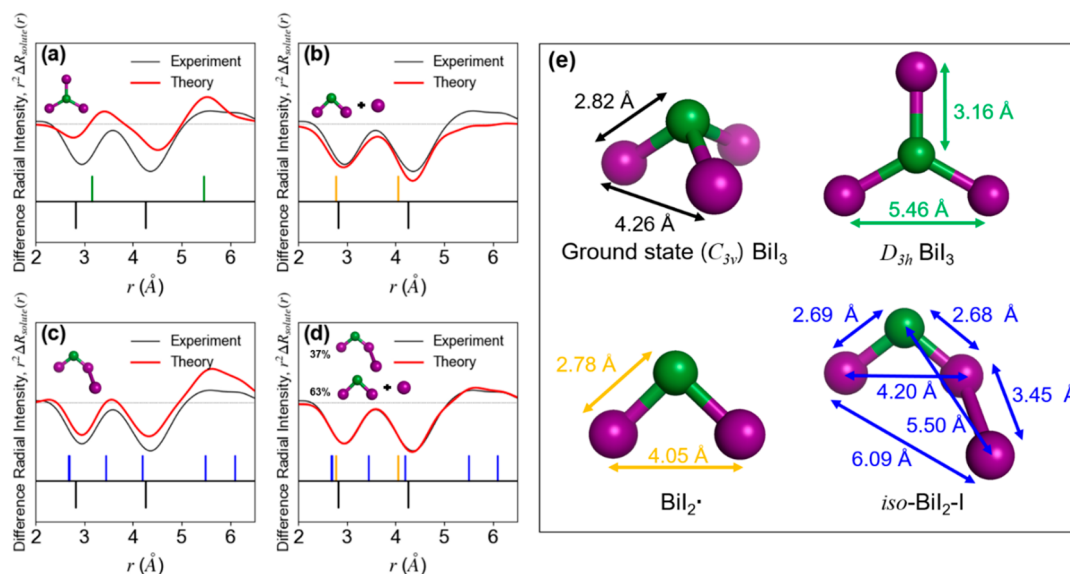


Figure 4. Experimental (black) and theoretical (red) solute-only difference radial intensities at 100 ps time delay for the candidate pathways of (a), trigonal planar BiI_3 with D_{3h} symmetry (b) dissociation fragments ($\text{BiI}_2\cdot + \text{I}\cdot$), (c) $\text{iso-BiI}_2\text{-I}$, and (d) a mixture of $\text{iso-BiI}_2\text{-I}$ and dissociation fragments ($\text{BiI}_2\cdot + \text{I}\cdot$). In each panel, the positions of the interatomic distances are shown with vertical bars. The upward and downward bars indicate the interatomic distances of the reaction products and the depleted ground state, respectively. The bars are colored according to the atom–atom pair distances in the chemical species relevant for the four candidate reaction pathways (that is, the ground-state BiI_3 with C_{3v} symmetry, trigonal planar BiI_3 with D_{3h} symmetry, $\text{BiI}_2\cdot$, and $\text{iso-BiI}_2\text{-I}$), as shown in panel (e).

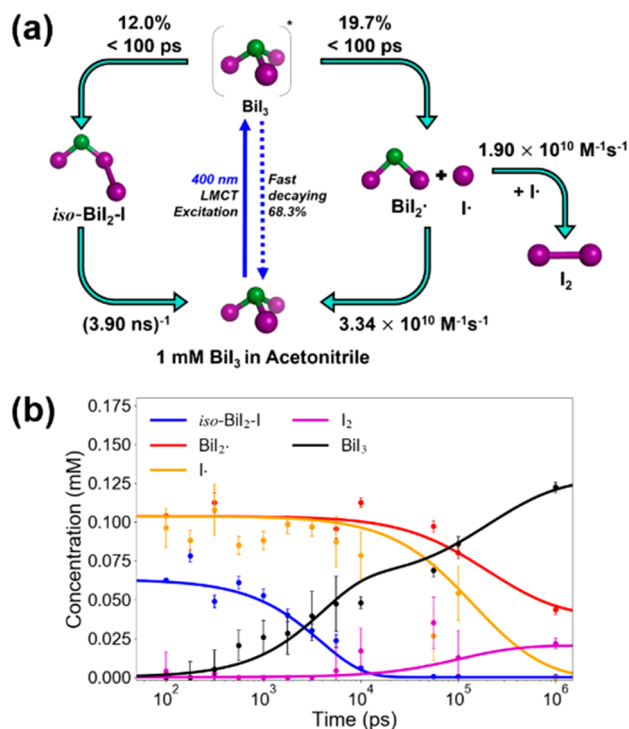


Figure 5. (a) Reaction mechanism of BiI_3 in acetonitrile upon 400 nm excitation. (b) Time-dependent concentration profiles for the reactant and photoproduct species determined by global fit analysis of TRXL data. Dots with error bars were obtained by fitting the individual experimental difference scattering curve at each time delay by a linear combination of necessary components, such as solute, cage, and solvent terms, and solid lines were obtained from the global fit analysis.

the I^- ligand to the $\text{I}\cdot$ radical. Subsequently, $68.3 \pm 1.5\%$ of the excited molecules rapidly relax back to the ground state while releasing a part of the photoexcitation energy as heat to

surrounding solvent molecules. Among the remaining $31.7 \pm 1.5\%$ of excited molecules, $12.0 \pm 0.6\%$ isomerize to form $\text{iso-BiI}_2\text{-I}$ and $19.7 \pm 1.0\%$ dissociate to yield $\text{BiI}_2\cdot$ and $\text{I}\cdot$ radicals. Because both of these reaction pathways occur faster than our temporal resolution (100 ps), the kinetic components corresponding to them are not identified from the TRXL data. The $\text{iso-BiI}_2\text{-I}$ isomer reverts back to the ground state with a time constant of 3.90 ± 0.41 ns. The dissociation fragments, $\text{BiI}_2\cdot$ and $\text{I}\cdot$, nongeminately recombine to form the ground state BiI_3 and molecular iodine with bimolecular rates of $3.34 (\pm 0.43) \times 10^{10} \text{ M}^{-1} \text{ s}^{-1}$ and $1.90 (\pm 0.48) \times 10^{10} \text{ M}^{-1} \text{ s}^{-1}$, respectively. These mixed processes of the fast unimolecular relaxation and the two slow bimolecular recombination reactions can also be identified from right singular vectors (RSVs) obtained from singular value decomposition (SVD) of the TRXL data in a high- q region, where the solute term is dominant. As can be seen in Figure S5, the RSVs for both the experimental and theoretical scattering curves are well described by a sum of two exponential functions, of which one is attributed to the fast unimolecular relaxation and the other describes the slow bimolecular reactions.

To confirm the validity of the reaction mechanism involving the two parallel pathways, we performed the geometry optimization of the ground electronic states of BiI_3 using density functional theory (DFT), and its results are illustrated in Tables S1 and S2. The ground-state BiI_3 has a pyramidal structure with a Bi–I bond of 2.826 Å length and two Bi–I bonds of 2.824 Å length. Because the two types of Bi–I bond lengths are different by only 0.002 Å, the ground-state BiI_3 can be regarded as belonging to the C_{3v} symmetry group, and we label it as $S_0\text{-}C_{3v}$. We also found the optimized structure of the isomer species, $\text{iso-BiI}_2\text{-I}$, in S_0 state and labeled it as $S_0\text{-iso}$. $S_0\text{-iso}$ is located at a shallow minimum with the energy of 1.73 eV relative to $S_0\text{-}C_{3v}$. From the calculated energies of (i) the transition state, $S_0\text{-TS}$, between $S_0\text{-iso}$ and $S_0\text{-}C_{3v}$ and (ii) the

dissociation fragments ($\text{BiI}_2\cdot + \text{I}\cdot$), the barrier from $S_0\text{-iso}$ to $S_0\text{-C}_{3v}$ is estimated to be only 0.06 eV and the energy required for dissociation into radicals should be at least 0.39 eV. Thus, after the formation of $S_0\text{-iso}$, the relaxation back to the ground state ($S_0\text{-C}_{3v}$) should be favored over the dissociation into the radical fragments, $\text{BiI}_2\cdot + \text{I}\cdot$. This result of DFT calculation on the energetics of S_0 is consistent with the optimal kinetic model, where $\text{iso-BiI}_2\text{-I}$ relaxes back to the ground state instead of being dissociated into radicals and the pathway of isomer formation is parallel with the dissociation pathway.

The optimized structural parameters of the reactant and photoproduct species determined from the TRXL experiment and DFT calculations are presented in Figure 6. Overall, the

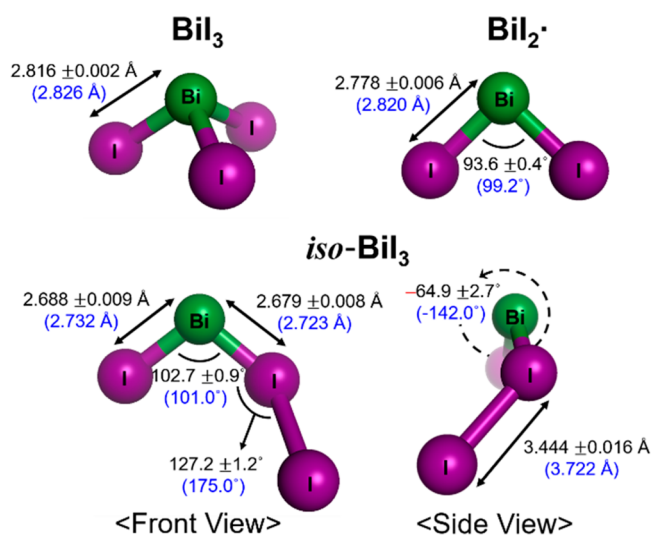


Figure 6. Comparison of structures of ground-state BiI_3 , $\text{iso-BiI}_2\text{-I}$, and $\text{BiI}_2\cdot$ determined from the experimental TRXL data and their DFT-optimized structures. The values of the bond lengths and bond angles determined from the global fit analysis of the TRXL data are shown in black font, and those from DFT calculations are shown in blue font in parentheses. For $\text{iso-BiI}_2\text{-I}$, the dihedral angle is also indicated by a dashed circular arrow in the lower right panel.

bond lengths obtained from the DFT calculations are overestimated by 0.3–1.6% compared with the experimentally determined values. Also, the dihedral angle of $\text{iso-BiI}_2\text{-I}$ was predicted to be -142.0° from the DFT calculation, in contrast to -64.9° determined from the TRXL experiment, meaning that the DFT-predicted geometry of $\text{iso-BiI}_2\text{-I}$ is more planar than the one determined by the TRXL experiment. We note that the structure of $\text{iso-BiI}_2\text{-I}$ strongly depends on the choice of DFT functional and the solvation field, which was also the case for $\text{iso-CHI}_2\text{-I}$, while the structure of BiI_3 is less sensitive to those factors, as listed in Tables S1 and S2. The dependence of optimized structure on DFT functional and the comparison of DFT-optimized and TRXL-determined structures are discussed in detail in the Supporting Information.

From the TRXL measurement, we found that photoexcited BiI_3 in acetonitrile undergoes two parallel reactions: (i) formation of $\text{iso-BiI}_2\text{-I}$ and (ii) dissociation into $\text{BiI}_2\cdot$ and $\text{I}\cdot$ radicals. The branching ratio between the isomer formation and the dissociation is 38:62 with an uncertainty of 3. In addition, the detailed structures of the photoproducts, $\text{iso-BiI}_2\text{-I}$ and $\text{BiI}_2\cdot$, were determined by virtue of structural sensitivity of TRXL. In particular, it should be noted that Bi–I bonds are shortened in both $\text{BiI}_2\cdot$ and $\text{iso-BiI}_2\text{-I}$ compared

with that in the ground-state BiI_3 . Such contraction of the Bi–I bond induced by the photoreaction is consistent with recent studies of other trihalides, AX_3 , where $\text{A} = \text{CH}$, B , or P and $\text{X} = \text{I}$ or Br . In addition, we note that the I–I bond (3.444 \AA) of $\text{iso-BiI}_2\text{-I}$ is considerably long, even longer than Bi–I bonds ($2.68\text{--}2.82 \text{ \AA}$), which are in principle expected to be longer than I–I bonds, of the reactant and photoproducts of BiI_3 , including $\text{BiI}_2\cdot$, and $\text{iso-BiI}_2\text{-I}$. The long X–X bond is a common structural feature of isomeric species of other trihalides. Especially, the I–I bond of $\text{iso-BiI}_2\text{-I}$ is significantly longer than that of other trihalide isomers. The halogen–halogen bond in isomeric species of various halocarbons has the character of polar covalent bond and therefore can be affected by the polar environment.³⁶ According to a study on CHBr_3 , it was theoretically shown that the structure of $\text{iso-CHBr}_2\text{-Br}$ varies depending on the solvent polarity, especially with the Br–Br bond length being proportional to the solvent polarity.³⁷ Accordingly, the I–I bond of $\text{iso-BiI}_2\text{-I}$ (3.444 \AA) is long in acetonitrile, which is a polar solvent, and especially much longer than the I–I bond of an isomer, $\text{iso-CHI}_2\text{-I}$, (2.922 \AA) formed from the photoreaction of CHI_3 in nonpolar cyclohexane, which was recently investigated using TRXL. In addition, according to the study on CHBr_3 , the lifetime of the isomeric species changes depending on the solvent polarity, from a few nanoseconds in polar solvents to microseconds in nonpolar solvents. Such solvent dependence of lifetime of the isomeric species can be attributed to the polar nature of the transition state between $\text{iso-BiI}_2\text{-I}$ and the ground state ($S_0\text{-C}_{3v}$) (see the Supporting Information and Table S2). Because the transition state can be stabilized with solvation by polar solvent molecules, the barrier for back isomerization to the ground state becomes smaller. In fact, $\text{iso-BiI}_2\text{-I}$ in (polar) acetonitrile (3.90 ns) exhibits much shorter lifetime than $\text{iso-CHI}_2\text{-I}$ in (nonpolar) cyclohexane (330 ns).

The TRXL data show no evidence for the formation of trigonal planar BiI_3 with D_{3h} symmetry, which is predicted to be the most stable structure in the S_1 state of BiI_3 . We propose that, at the earliest stage of the photoreaction, the trigonal planar BiI_3 with D_{3h} symmetry may serve as a primary reaction intermediate that branches into the two reaction pathways, that is, the formation of $\text{iso-BiI}_2\text{-I}$ and the dissociation fragments.

In this work, we investigated the spatiotemporal kinetics of photoinduced reaction of BiI_3 in solution. By analyzing the time-dependent X-ray scattering signals, we identified the kinetics and structures of major intermediate species. We also performed DFT/TDDFT quantum calculations for BiI_3 , which support our experimental findings. Interestingly, trigonal planar BiI_3 with D_{3h} symmetry is predicted as the optimum structure of S_1 according to our calculation, but it was not observed from the analysis of our TRXL data. This stable form of BiI_3 may be the primary intermediate formed at the earliest stage of the reaction. It should be feasible to directly observe the evolution dynamics of this primary intermediate with ultrafast optical spectroscopy or femtosecond X-ray scattering using an X-ray free electron laser (XFEL). The present contribution may initiate further studies of BiI_3 and related trihalide/metal halide systems, which will enable us to extend our understanding of the underlying reaction mechanism of those systems.

■ ASSOCIATED CONTENT

Supporting Information

The Supporting Information is available free of charge on the ACS Publications website at DOI: 10.1021/acs.jpcllett.9b00365.

Details of TRXL experiment, data processing, data analysis, density functional theory calculation, and molecular dynamics simulation; decomposition of solution scattering signal, $q\Delta S(q, t)$ and $r^2\Delta R(r, t)$; experimental solute-only $r^2\Delta R(r, t)$; SVD analysis of experimental, theoretical, and mock data; polychromatic correction; DFT-optimized versus experimentally determined structures of BiI_3 , BiI_2^- , and *iso*- BiI_2^- -I (PDF)

■ AUTHOR INFORMATION

Corresponding Author

*E-mail: hyotcherl.ihce@kaist.ac.kr

ORCID

Eun Hyuk Choi: 0000-0001-9051-9946

Doo-Sik Ahn: 0000-0001-9154-1029

Tae Wu Kim: 0000-0002-6370-0907

Hosung Ki: 0000-0001-8273-6596

Jungkweon Choi: 0000-0002-9979-305X

Martin Nors Pedersen: 0000-0001-6975-5071

Jeongho Kim: 0000-0003-4085-293X

Hyotcherl Ihce: 0000-0003-0397-5965

Author Contributions

[†]E.H.C. and D.-S.A. contributed equally to this work.

Notes

The authors declare no competing financial interest.

■ ACKNOWLEDGMENTS

This work was supported by Institute for Basic Science (IBS-R004).

■ REFERENCES

- Andris, E.; Andrikopoulos, P. C.; Schulz, J.; Turek, J.; Ruzicka, A.; Roithova, J.; Rulisek, L. Auophilic Interactions in [(L)AuCl]...[(L)AuCl] Dimers: Calibration by Experiment and Theory. *J. Am. Chem. Soc.* **2018**, *140*, 2316–2325.
- Hickey, D. P.; Sandford, C.; Rhodes, Z.; Gensch, T.; Fries, L. R.; Sigman, M. S.; Minter, S. D. Investigating the Role of Ligand Electronics on Stabilizing Electrochemically Relevant Low-Valent Co(I) Intermediates. *J. Am. Chem. Soc.* **2019**, *141*, 1382–1392.
- Zhang, W. K.; Kjaer, K. S.; Alonso-Mori, R.; Bergmann, U.; Chollet, M.; Fredin, L. A.; Hadt, R. G.; Hartsock, R. W.; Harlang, T.; Kroll, T.; Kubicek, K.; Lemke, H. T.; Liang, H. W.; Liu, Y. Z.; Nielsen, M. M.; Persson, P.; Robinson, J. S.; Solomon, E. I.; Sun, Z.; Sokaras, D.; van Driel, T. B.; Weng, T. C.; Zhu, D. L.; Warnmark, K.; Sundström, V.; Gaffney, K. J. Manipulating charge transfer excited state relaxation and spin crossover in iron coordination complexes with ligand substitution. *Chemical Science* **2017**, *8*, 515–523.
- Carbery, W. P.; Verma, A.; Turner, D. B. Spin-Orbit Coupling Drives Femtosecond Nonadiabatic Dynamics in a Transition Metal Compound. *J. Phys. Chem. Lett.* **2017**, *8*, 1315–1322.
- Shields, B. J.; Kudisch, B.; Scholes, G. D.; Doyle, A. G. Long-Lived Charge-Transfer States of Nickel(II) Aryl Halide Complexes Facilitate Bimolecular Photoinduced Electron Transfer. *J. Am. Chem. Soc.* **2018**, *140*, 3035–3039.
- Glebov, E. M.; Kolomeets, A. V.; Pozdnyakov, I. P.; Plyusnin, V. F.; Grivin, V. P.; Tkachenko, N. V.; Lemmetyinen, H. Redox processes in photochemistry of Pt(IV) hexahaloid complexes. *RSC Adv.* **2012**, *2*, 5768–5778.
- Glebov, E. M.; Pozdnyakov, I. P.; Plyusnin, V. F.; Khmelinskii, I. Primary reactions in the photochemistry of hexahalide complexes of platinum group metals: A minireview. *J. Photochem. Photobiol., C* **2015**, *24*, 1–15.
- Smeigh, A. L.; Katz, J. E.; Brunschwig, B. S.; Lewis, N. S.; McCusker, J. K. Effect of the presence of iodide on the electron injection dynamics of dye-sensitized TiO₂-based solar cells. *J. Phys. Chem. C* **2008**, *112*, 12065–12068.
- Rack, J. J.; Gray, H. B. Spectroscopy and electrochemistry of mer-[RuCl₃(dmsol)(tmen)]. Dimethylsulfoxide is sulfur-bonded to Ru(II), Ru(III), and Ru(IV). *Inorg. Chem.* **1999**, *38*, 2–3.
- Hoefler, S. F.; Trimmel, G.; Rath, T. Progress on lead-free metal halide perovskites for photovoltaic applications: a review. *Monatsh. Chem.* **2017**, *148*, 795–826.
- Williamson, B. W.; Eickemeyer, F. T.; Hillhouse, H. W. Solution-Processed BiI₃ Films with 1.1 eV Quasi-Fermi Level Splitting: The Role of Water, Temperature, and Solvent during Processing. *ACS Omega* **2018**, *3*, 12713–12721.
- Hamdeh, U. H.; Nelson, R. D.; Ryan, B. J.; Bhattacharjee, U.; Petrich, J. W.; Panthani, M. G. Solution-Processed BiI₃ Thin Films for Photovoltaic Applications: Improved Carrier Collection via Solvent Annealing. *Chem. Mater.* **2016**, *28*, 6567–6574.
- Lehner, A. J.; Wang, H. B.; Fabiani, D. H.; Liman, C. D.; Hebert, C. A.; Perry, E. E.; Wang, M.; Bazan, G. C.; Chabynyc, M. L.; Seshadri, R. Electronic structure and photovoltaic application of BiI₃. *Appl. Phys. Lett.* **2015**, *107*, 131109.
- Brandt, R. E.; Kurchin, R. C.; Hoyer, R. L. Z.; Poindexter, J. R.; Wilson, M. W. B.; Sulekar, S.; Lenahan, F.; Yen, P. X. T.; Stevanovic, V.; Nino, J. C.; Bawendi, M. G.; Buonassisi, T. Investigation of Bismuth Triiodide (BiI₃) for Photovoltaic Applications. *J. Phys. Chem. Lett.* **2015**, *6*, 4297–4302.
- Ollevier, T. New trends in bismuth-catalyzed synthetic transformations. *Org. Biomol. Chem.* **2013**, *11*, 2740–2755.
- Vidal, S. Bismuth(III) derivatives: New catalysts. *Synlett* **2001**, *2001*, 1194–1195.
- Molnar, J.; Kolonits, M.; Hargittai, M.; Konings, R. J. M.; Booij, A. S. Molecular structure of SbI₃ and BiI₃ from combined electron diffraction and vibrational spectroscopic studies. *Inorg. Chem.* **1996**, *35*, 7639–7642.
- Scholz, M.; Oum, K.; Lenzer, T. Pronounced exciton and coherent phonon dynamics in BiI₃. *Phys. Chem. Chem. Phys.* **2018**, *20*, 10677–10685.
- Horvath, O.; Miko, I. Spectra, equilibrium and photoredox chemistry of iodobismuthate(III) complexes in acetonitrile. *Inorg. Chim. Acta* **2000**, *304*, 210–218.
- Oldenburg, K.; Vogler, A.; Miko, I.; Horvath, O. Photoredox decomposition of tin(II), lead(II), antimony(III) and bismuth(III) iodide complexes in solution. *Inorg. Chim. Acta* **1996**, *248*, 107–110.
- Wall, M.; Tarnovsky, A. N.; Pascher, T.; Sundstrom, V.; Akesson, E. Photodissociation dynamics of iodoform in solution. *J. Phys. Chem. A* **2003**, *107*, 211–217.
- Maurer, A. B.; Hu, K.; Meyer, G. J. Light Excitation of a Bismuth Iodide Complex Initiates I-I Bond Formation Reactions of Relevance to Solar Energy Conversion. *J. Am. Chem. Soc.* **2017**, *139*, 8066–8069.
- Kim, J.; Lee, J. H.; Kim, J.; Jun, S.; Kim, K. H.; Kim, T. W.; Wulff, M.; Ihce, H. Structural Dynamics of 1,2-Diiodoethane in Cyclohexane Probed by Picosecond X-ray Liquidography. *J. Phys. Chem. A* **2012**, *116*, 2713–2722.
- Anderson, C. P.; Spears, K. G.; Wilson, K. R.; Senson, R. J. Solvent dependent branching between C-I and C-Br bond cleavage following 266 nm excitation of CH₂BrI. *J. Chem. Phys.* **2013**, *139*, 194307.
- Tarnovsky, A. N.; Sundstrom, V.; Akesson, E.; Pascher, T. Photochemistry of diiodomethane in solution studied by femtosecond and nanosecond laser photolysis. Formation and dark reactions of the CH₂I-I isomer photoproduct and its role in cyclopropanation of olefins. *J. Phys. Chem. A* **2004**, *108*, 237–249.

(26) Mereshchenko, A. S.; Butaeva, E. V.; Borin, V. A.; Eyzips, A.; Tarnovsky, A. N. Roaming-mediated ultrafast isomerization of geminal tri-bromides in the gas and liquid phases. *Nat. Chem.* **2015**, *7*, 562–568.

(27) Christensen, M.; Haldrup, K.; Bechgaard, K.; Feidenhans'l, R.; Kong, Q. Y.; Cammarata, M.; Russo, M. L.; Wulff, M.; Harrit, N.; Nielsen, M. M. Time-Resolved X-ray Scattering of an Electronically Excited State in Solution. Structure of the $^3A_{2u}$ State of Tetrakis-mu-pyrophosphitodiplatinate(II). *J. Am. Chem. Soc.* **2009**, *131*, 502–508.

(28) Haldrup, K.; Harlang, T.; Christensen, M.; Dohn, A.; van Driel, T. B.; Kjaer, K. S.; Harrit, N.; Vibenholt, J.; Guerin, L.; Wulff, M.; Nielsen, M. M. Bond Shortening (1.4 Å) in the Singlet and Triplet Excited States of $[\text{Ir}_2(\text{dimen})_4]^{2+}$ in Solution Determined by Time-Resolved X-ray Scattering. *Inorg. Chem.* **2011**, *50*, 9329–9336.

(29) Rimmerman, D.; Leshchev, D.; Hsu, D. J.; Hong, J. Y.; Abraham, B.; Kosheleva, I.; Henning, R.; Chen, L. X. Insulin hexamer dissociation dynamics revealed by photoinduced T-jumps and time-resolved X-ray solution scattering. *Photochemical & Photobiological Sciences* **2018**, *17*, 874–882.

(30) Kim, K. H.; Kim, J. G.; Nozawa, S.; Sato, T.; Oang, K. Y.; Kim, T.; Ki, H.; Jo, J.; Park, S.; Song, C.; Sato, T.; Ogawa, K.; Togashi, T.; Tono, K.; Yabashi, M.; Ishikawa, T.; Kim, J.; Ryoo, R.; Kim, J.; Ihee, H.; Adachi, S. Direct observation of bond formation in solution with femtosecond X-ray scattering. *Nature* **2015**, *518*, 385–389.

(31) Ihee, H.; Lorenc, M.; Kim, T. K.; Kong, Q. Y.; Cammarata, M.; Lee, J. H.; Bratos, S.; Wulff, M. Ultrafast x-ray diffraction of transient molecular structures in solution. *Science* **2005**, *309*, 1223–1227.

(32) Ahn, C. W.; Ki, H.; Kim, J.; Kim, J.; Park, S.; Lee, Y.; Kim, K. H.; Kong, Q. Y.; Moon, J.; Pedersen, M. N.; Wulff, M.; Ihee, H. Direct Observation of a Transiently Formed Isomer During Iodoform Photolysis in Solution by Time-Resolved X-ray Liquidography. *J. Phys. Chem. Lett.* **2018**, *9*, 647–653.

(33) Marcellini, M.; Nasedkin, A.; Zietz, B.; Petersson, J.; Vincent, J.; Palazzetti, F.; Malmerberg, E.; Kong, Q. Y.; Wulff, M.; van der Spoel, D.; Neutze, R.; Davidsson, J. Transient isomers in the photo-dissociation of bromiodomethane. *J. Chem. Phys.* **2018**, *148*, 134307.

(34) Ki, H.; Oang, K. Y.; Kim, J.; Ihee, H. Ultrafast X-Ray Crystallography and Liquidography. *Annu. Rev. Phys. Chem.* **2017**, *68*, 473–497.

(35) Ihee, H.; Wulff, M.; Kim, J.; Adachi, S. Ultrafast X-ray scattering: structural dynamics from diatomic to protein molecules. *Int. Rev. Phys. Chem.* **2010**, *29*, 453–520.

(36) Borin, V. A.; Matveev, S. M.; Budkina, D. S.; El-Khoury, P. Z.; Tarnovsky, A. N. Direct photoisomerization of CH_2I_2 vs. CHBr_3 in the gas phase: a joint 50 fs experimental and multireference resonance-theoretical study. *Phys. Chem. Chem. Phys.* **2016**, *18*, 28883–28892.

(37) Pal, S. K.; Mereshchenko, A. S.; Butaeva, E. V.; El-Khoury, P. Z.; Tarnovsky, A. N. Global sampling of the photochemical reaction paths of bromoform by ultrafast deep-UV through near-IR transient absorption and ab initio multiconfigurational calculations. *J. Chem. Phys.* **2013**, *138*, 124501.